Eur. Phys. J. B **73**, 117–124 (2010)
DOI: 10.1140/epjb/e2009-00400-4

THE EUROPEAN PHYSICAL JOURNAL B

Regular Article

The spin-1/2 J_1–J_2 Heisenberg antiferromagnet on the square lattice: Exact diagonalization for N = 40 spins

J. Richter[1,a] and J. Schulenburg[2]

[1] Institut für Theoretische Physik, Universität Magdeburg, 39016 Magdeburg, Germany
[2] Universitätsrechenzentrum, Universität Magdeburg, 39016 Magdeburg, Germany

Received 18 September 2009
Published online 25 November 2009 –

Abstract. We present numerical exact results for the ground state and the low-lying excitations for the spin-1/2 J_1–J_2 Heisenberg antiferromagnet on finite square lattices of up to $N = 40$ sites. Using finite-size extrapolation we determine the ground-state energy, the magnetic order parameters, the spin gap, the uniform susceptibility, as well as the spin-wave velocity and the spin stiffness as functions of the frustration parameter J_2/J_1. In agreement with the generally excepted scenario we find semiclassical magnetically ordered phases for $J_2 < J_2^{c1}$ and $J_2 > J_2^{c2}$ separated by a gapful quantum paramagnetic phase. We estimate $J_2^{c1} \approx 0.35 J_1$ and $J_2^{c2} \approx 0.66 J_1$.

PACS. 75.10.Jm Quantized spin models – 75.45.+j Macroscopic quantum phenomena in magnetic systems

1 Introduction

The spin-1/2 Heisenberg antiferromagnet (HAFM) with nearest-neighbor (NN) J_1 and frustrating next-nearest-neighbor (NNN) J_2 coupling (J_1–J_2 model) on the square lattice has attracted a great deal of interest during the last twenty years (see, e.g., Refs. [1–35] and references therein). The corresponding Hamiltonian reads

$$H = J_1 \sum_{\langle i,j \rangle} \mathbf{s}_i \cdot \mathbf{s}_j + J_2 \sum_{\langle\langle i,k \rangle\rangle} \mathbf{s}_i \cdot \mathbf{s}_j, \qquad (1)$$

where the sums over $\langle i,j \rangle$ and $\langle\langle i,k \rangle\rangle$ run over all NN and NNN pairs, respectively, counting each bond once. In what follows we set $J_1 = 1$. The synthesis of layered magnetic materials [37,38] which can be described by the spin-1/2 J_1–J_2 model has stimulated a renewed interest in this model. Another new promising perspective is also opened by the recently discovered layered Fe-based superconducting materials [39] which may have a magnetic phase that can be described by a J_1–J_2 model with spin quantum number $s > 1/2$ [40–42].

The J_1–J_2 model is a canonical model to study quantum phase transitions between semiclassical magnetically ordered ground state (GS) phases and novel non-magnetic quantum phases. Moreover, the J_1–J_2 model might be also a candidate for a deconfined critical point separating a semiclassical magnetic phase from non-magnetic quantum phase [21,31,32,43,44].

Due to frustration highly efficient quantum Monte-Carlo codes [45], such as the stochastic series expansion suffer from the minus sign problem. Therefore, many other approximate methods, e.g., the Green's function method [16,23], the series expansion [14,17,19,21,32], the Schwinger boson approach [11], the coupled cluster method [13,23,30,31], variational techniques [18,34], the path integral quantization [24], the cluster effective-field theory [25,28], the hierarchical mean-field approach [29], the projected entangled pair states method [35] as well as the stochastic state selection method [27] were used to find the GS phases of the model. One of the most powerful methods is the Lanczos exact diagonalization method which yields numerically exact results for finite lattices. It has been succesfully applied to the J_1–J_2 model in various papers, see, e.g., references [2,3,5,7–10,12,15,22]. In particular, the paper of Schulz and coworkers [5] presenting for the first time results for lattices up to $N = 36$ sites has set a benchmark for such studies and provides detailed information on the model. In addition, these numerical exact results are often used to test new approximate methods, see, e.g., references [27,31,36].

Due to the progress in the computer hardware and also to the increase in the efficiency in programming the Lanczos algorithm, very recently the GS and low-lying excitations of the unfrustrated (i.e., $J_2 = 0$) spin-1/2 HAFM [46] and of a spin-1/2 Heisenberg model with ring exchange [47] have been calculated for a square lattice with $N = 40$ sites. The largest two-dimensional quantum spin model for which the GS has been calculated so far is the spin-1/2 HAFM on the star lattice with $N = 42$

[a] e-mail: johannes.richter@physik.uni-magdeburg.de

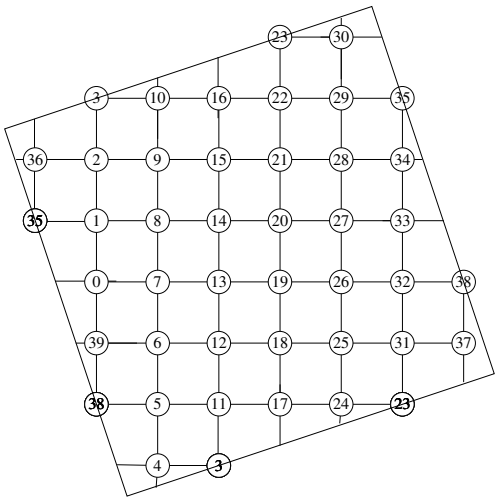

Fig. 1. The finite square lattice with $N = 40$ sites.

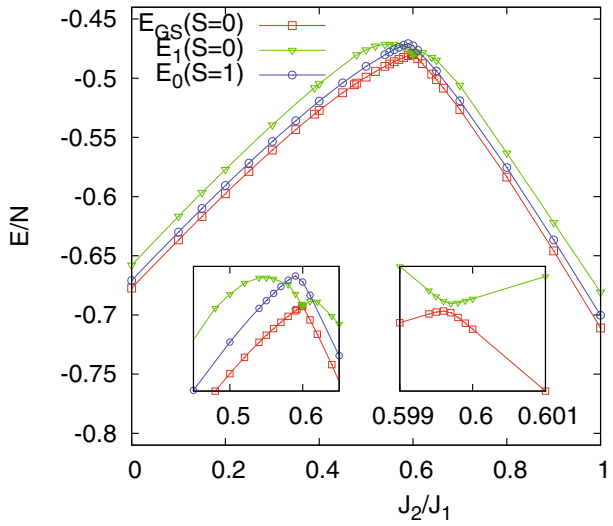

Fig. 2. (Color online) Singlet GS energy, $E_{GS}(S = 0)$, the energy of the first triplet excitation, $E_0(S = 1)$, and the energy of the first singlet excitation, $E_1(S = 0)$, versus J_2 for the square lattice with $N = 40$ sites.

sites [48]. Note, however, that for higher sectors of S_z which are relevant for finite magnetic fields much larger system sizes can be considered, see, e.g., reference [49].

As a result of numerous investigations it seems to be clear now that the J_1–J_2 model exhibits two magnetically long-range ordered phases at small and at large J_2 separated by an intermediate quantum paramagnetic phase without magnetic long-range order (LRO) in the parameter region $J_2^{c1} < J_2 < J_2^{c2}$, where $J_2^{c1} \approx 0.4J_1$ and $J_2^{c2} \approx 0.6J_1$. The GS at low $J_2 < J_2^{c1}$ exhibits semiclassical Néel magnetic LRO with the magnetic wave vector $\mathbf{Q}_0 = (\pi, \pi)$. The GS at large $J_2 > J_2^{c2}$ shows so-called collinear magnetic LRO with the magnetic wave vectors $\mathbf{Q}_1 = (\pi, 0)$ or $\mathbf{Q}_2 = (0, \pi)$. These two collinear states are characterized by a parallel spin orientation of nearest neighbors in vertical (horizontal) direction and an antiparallel spin orientation of nearest neighbors in horizontal (vertical) direction.

The nature of the transition between the Néel and the quantum paramagnetic phase as well as the properties of the quantum paramagnetic phase and the precise values of the transition points are still under discussion [1–3,5–10,13–32,34].

In this paper we present new results for the GS and the low-lying excitations of the J_1–J_2 model for a finite lattice of $N = 40$ sites shown as in Figure 1. These results are presented in detail, on the one hand, as benchmark data for approximate methods. On the other hand, we combine our new results with the known results [5] (which we have recalculated) to improve the finite-size extrapolation. For all the finite lattices periodic boundary conditions were imposed.

2 Results of Lanczos exact diagonalization for a finite square lattice of N = 40 sites

Although Schulz and coworkers performed the Lanczos diagonalization for the spin-1/2 J_1–J_2 HAFM on the finite square lattice of $N = 36$ sites more then 10 years ago the corresponding Lanczos diagonalization for the finite lattice of $N = 40$ sites is still a challenging problem. The number of basis states on the square lattice in the GS symmetry sector is $n_h = 430\,909\,650$ for $N = 40$ compared to $n_h = 15\,804\,956$ for $N = 36$. The GS belongs to a translational symmetry with $\mathbf{q} = (0, 0)$.

The most important quantities in order to analyze semiclassical GS magnetic ordering are appropriate order parameters corresponding to the classical Néel and collinear LRO. Following Schulz et al. [5] we use here the $\mathbf{Q}$-dependent susceptibilities (square of order parameters) defined as

$$M_N^2(\mathbf{Q}) = \frac{1}{N(N+2)} \sum_{i,j} \langle \mathbf{s}_i \cdot \mathbf{s}_j \rangle e^{i\mathbf{Q}(\mathbf{R}_i - \mathbf{R}_j)}. \quad (2)$$

For the magnetic wave vector $\mathbf{Q}_0 = (\pi, \pi)$ the quantity $M_N^2(\mathbf{Q_0})$ is the relevant order parameter for the Néel ordered GS phase present at small J_2, whereas $M_N^2(\mathbf{Q_{1(2)}})$ with magnetic wave vectors $\mathbf{Q}_1 = (\pi, 0)$ or $\mathbf{Q}_2 = (0, \pi)$ corresponds to the collinear magnetic LRO present at large J_2.

In Table 1 we give the singlet GS energy, $E_{GS}(S = 0)$, the energy of the first triplet excitation $E_0(S = 1)$, the energy of the first singlet excitation $E_1(S = 0)$, as well as the $\mathbf{Q}$-dependent susceptibilities $M_N^2(\pi, \pi)$, $M_N^2(\pi, 0)$. The low-lying energies are also displayed in Figure 2 where more data points are included than shown in Table 1. It is obvious that the first excited singlet state becomes very close to the singlet GS near $J_2 = 0.6$. Since both states belong to the same lattice symmetry, a level crossing is forbidden due to the von Neumann-Wigner theorem [50]. The numerical data shown in the right inset of Figure 2 clearly give a numerical check of this general theorem. The energies of the low-lying states show the typical frustration induced maximum known from previous ED calculations for smaller lattices, see, e.g., references [2,5,7]. Since we

Table 1. Ground state energy $E_{GS}(S=0)$, first triplet excitation energy $E_0(S=1)$, first singlet excitation energy $E_1(S=0)$, square of Néel order parameter $M_N^2(\pi,\pi)$ and square of collinear order parameter $M_N^2(\pi,0)$.

J_2	$E_{GS}(S=0)$	$E_0(S=1)$	$E_1(S=0)$	$M_N^2(\pi,\pi)$	$M_N^2(\pi,0)$
0.0	–27.09485025	–26.83322962	–26.3138435	0.193923	0.011956
0.10	–25.46460260	–25.19683764	–24.6669636	0.184079	0.011994
0.20	–23.90046918	–23.62413648	–23.0809149	0.171482	0.012066
0.30	–22.42728643	–22.13740165	–21.5763396	0.154648	0.012212
0.40	–21.08836670	–20.77332213	–20.1877770	0.130935	0.012547
0.50	–19.96304839	–19.59762345	–19.0413364	0.097703	0.013446
0.55	–19.51791526	–19.11727950	–18.8522256	0.079043	0.014457
0.60	–19.18368038	–18.90110215	–19.1762893	0.020304	0.078160
0.65	–20.04603255	–19.75459787	–19.3898477	0.013516	0.093232
0.70	–21.05530239	–20.75925837	–20.2366849	0.010120	0.101552
0.80	–23.34020427	–23.01691919	–22.5277370	0.005522	0.111045
0.90	–25.83691287	–25.46196339	–24.8738325	0.002912	0.115628
1.00	–28.43880892	–28.00735838	–27.2299736	0.001700	0.117879

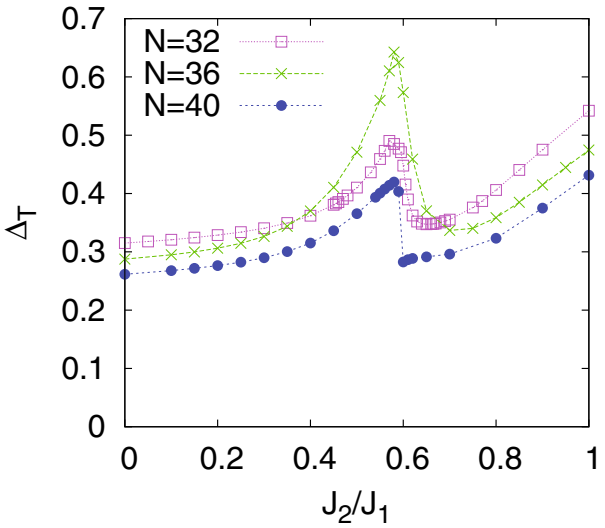

Fig. 3. (Color online) Spin gap $\Delta_T = E_{GS}(S=1) - E_0(S=0)$ versus J_2 for $N = 32$, 36, and 40.

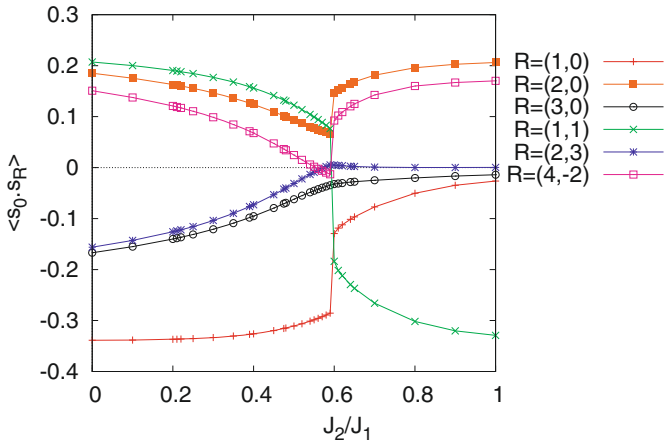

Fig. 4. (Color online) Selected spin-spin correlation functions $\langle \mathbf{s}_0 \cdot \mathbf{s}_\mathbf{R} \rangle$ for $N = 40$.

have data for the singlet GS and the first triplet excitation, we can also give results for the spin gap $\Delta_T = E_0(S = 1) - E_{GS}(S = 0)$, see Figure 3. Note that the spin gap was not presented in the paper of Schulz et al. [5]. Hence we compare in Figure 3 spin gap data for $N = 32$, 36, and 40. It is obvious that with increasing J_2 the gap starts to grow at $J_2 \approx 0.4J_1$. It reaches a maximum at about $J_2 \approx 0.58J_1$ and becomes again small for $J_2 \gtrsim 0.6J_1$. This behavior yields an indication of a gapful quantum paramagnetic GS phase around $J_2 = 0.5J_1$. However, it is also obvious that there is no monotonous finite-size behavior in that parameter region, i.e., a reliable finite-size extrapolation of the spin gap around $J_2 = 0.5J_1$ is not possible.

Next we consider the spin-spin correlation functions $\langle \mathbf{s}_0 \cdot \mathbf{s}_\mathbf{R} \rangle$. There are altogether 11 different correlations functions given in Table 2 for the same data points as in Table 1. Graphically the variation of some selected correlation functions are shown in Figure 4. For small J_2 the spin-spin correlations are quite strong and according to the Néel order we have $\langle \mathbf{s}_0 \cdot \mathbf{s}_\mathbf{R} \rangle < 0$ for $\mathbf{R}$ connecting sites of sublattices A and B but $\langle \mathbf{s}_0 \cdot \mathbf{s}_\mathbf{R} \rangle > 0$ for $\mathbf{R}$ connecting sites within a sublattice. Increasing the frustration leads to a weakening of the spin-spin correlation. This weakening is particularly strong for larger separations. For strong frustration around $J_2 = 0.5J_1$ all correlation functions $\langle \mathbf{s}_0 \cdot \mathbf{s}_\mathbf{R} \rangle$ except for $\mathbf{R} = (1,0)$; $(1,1)$; $(2,0)$ are very small which is an indication for a magnetically disordered phase. Beyond $J_2 \approx 0.6J_1$ the increasing strength of correlation functions for lattice vectors $\mathbf{R}$ connecting sites within the same sublattice A (or B) indicates the emerging collinear LRO. The corresponding order parameters defined in equation (2) and listed in Table 1 are shown in Figure 5. The suppression of magnetic order around $J_2 = 0.5J_1$ is again obvious. Although there is no level crossing (see the discussion above) we observe in Figures 4 and 5 a sharp change of the magnetic quantities near $J_2 = 0.6J_1$, i.e., at that point where both singlet levels become very close to each other (see Fig. 2, right inset). This behavior might be a hint on a first-order transition between the phase with collinear

Table 2. Spin-spin correlation function $\langle \mathbf{s}_0 \cdot \mathbf{s}_\mathbf{R} \rangle$ (respectively, $\langle \mathbf{s}_0 \cdot \mathbf{s}_i \rangle$, see Fig. 1)

	$\langle \mathbf{s}_0 \cdot \mathbf{s}_1 \rangle$	$\langle \mathbf{s}_0 \cdot \mathbf{s}_2 \rangle$	$\langle \mathbf{s}_0 \cdot \mathbf{s}_3 \rangle$	$\langle \mathbf{s}_0 \cdot \mathbf{s}_4 \rangle$	$\langle \mathbf{s}_0 \cdot \mathbf{s}_5 \rangle$	$\langle \mathbf{s}_0 \cdot \mathbf{s}_6 \rangle$	$\langle \mathbf{s}_0 \cdot \mathbf{s}_9 \rangle$	$\langle \mathbf{s}_0 \cdot \mathbf{s}_{10} \rangle$	$\langle \mathbf{s}_0 \cdot \mathbf{s}_{11} \rangle$	$\langle \mathbf{s}_0 \cdot \mathbf{s}_{16} \rangle$	$\langle \mathbf{s}_0 \cdot \mathbf{s}_{24} \rangle$
J_2	$\mathbf{R} = (1,0)$	$\mathbf{R} = (2,0)$	$\mathbf{R} = (3,0)$	$\mathbf{R} = (3,1)$	$\mathbf{R} = (2,1)$	$\mathbf{R} = (1,1)$	$\mathbf{R} = (1,2)$	$\mathbf{R} = (1,3)$	$\mathbf{R} = (2,2)$	$\mathbf{R} = (2,3)$	$\mathbf{R} = (4,-2)$
0.0	–0.338685	0.185133	–0.166989	0.164100	–0.179037	0.207198	–0.177165	0.157032	0.161478	–0.156222	0.150825
0.10	–0.338313	0.175458	–0.154968	0.151833	–0.166128	0.200046	–0.164196	0.144276	0.148815	–0.142812	0.137613
0.20	–0.336852	0.163089	–0.140055	0.136281	–0.149688	0.190488	–0.147774	0.128166	0.132678	–0.125913	0.120888
0.30	–0.333423	0.146655	–0.120879	0.115776	–0.127803	0.176943	–0.126123	0.107007	0.111225	–0.103674	0.098736
0.40	–0.326073	0.123909	–0.095208	0.087441	–0.097056	0.156171	–0.096186	0.077940	0.081246	–0.072885	0.067683
0.50	–0.310788	0.093354	–0.061983	0.048666	–0.053772	0.122499	–0.055281	0.039045	0.040050	–0.031119	0.024636
0.55	–0.298596	0.077397	–0.045300	0.027102	–0.028947	0.099315	–0.032856	0.018723	0.018048	–0.009279	0.001776
0.60	–0.129468	0.145560	–0.032355	–0.127482	0.034386	–0.183879	0.015885	–0.109425	0.107499	0.004956	0.092322
0.65	–0.096630	0.168312	–0.027747	–0.156408	0.033291	–0.236841	0.017844	–0.138945	0.137898	0.002280	0.124962
0.70	–0.077052	0.181365	–0.024825	–0.170640	0.030228	–0.265914	0.017595	–0.155349	0.155199	0.000924	0.142587
0.80	–0.050388	0.195918	–0.020247	–0.186357	0.025323	–0.301704	0.016110	–0.173610	0.174066	0.000216	0.159999
0.90	–0.034740	0.202785	–0.016548	–0.193845	0.021465	–0.320247	0.014244	–0.182238	0.182661	0.000291	0.166980
1.00	–0.026295	0.206295	–0.013959	–0.197463	0.018474	–0.329190	0.012522	–0.186480	0.186960	0.000333	0.170301

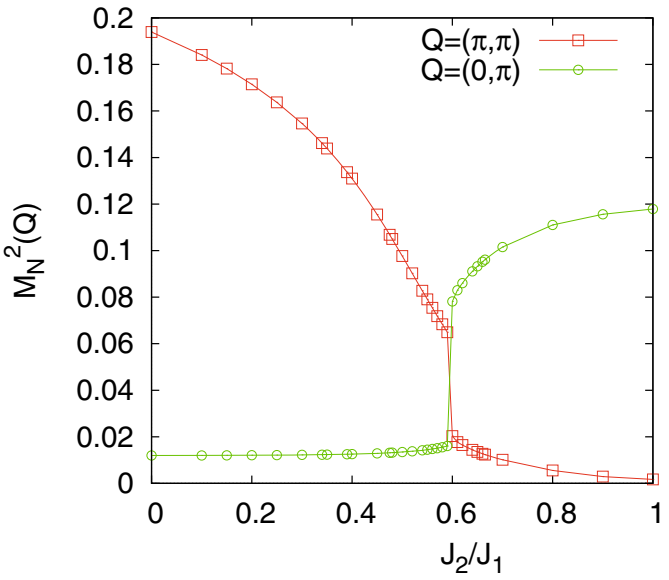

Fig. 5. (Color online) Square of order parameters $M_N^2(\mathbf{Q})$ for $\mathbf{Q} = (\pi, \pi)$ and $\mathbf{Q} = (0, \pi)$, see equation (2).

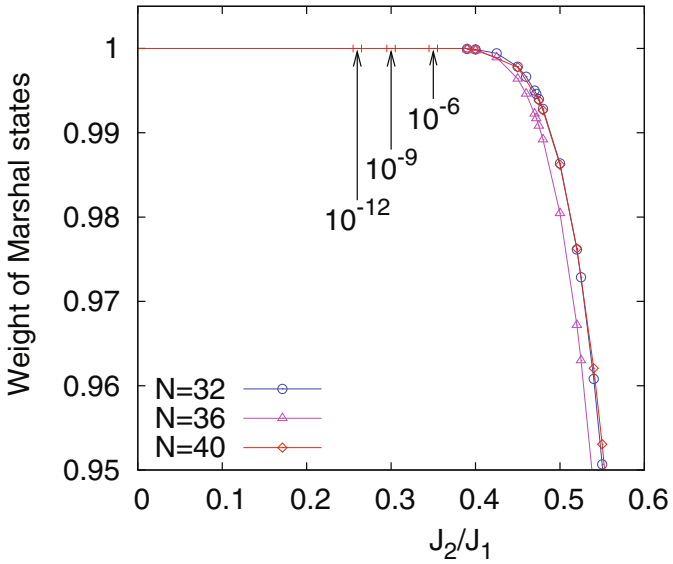

Fig. 6. (Color online) Validity of the MPSR: The curve shows the weight of the states fulfilling the MPSR, i.e., $\sum_n' |c_n|^2$ (where the sum $\sum'$ runs over those states only, for which the sign of c_n fulfills the MPSR). The arrows indicate those J_2 values for $N = 40$, where the weight of the states which do not fulfill the MPSR is 10^{-12}, 10^{-9} and 10^{-6}, respectively.

LRO and the magnetically disordered phase, see also, e.g., references [5,14,17,23,31].

Another interesting point is the breakdown of the Marshall-Peierls sign rule (MPSR) at $J_2 \approx 0.4 J_1$. Writing the GS as $|\Psi\rangle = \sum_n c_n |n\rangle$, where $|n\rangle$ is an Ising basis state of typical form $|\uparrow\uparrow\downarrow\uparrow\downarrow\downarrow \cdots\rangle$, the MPSR determines the sign of the coefficients c_n [51]. The MPSR has been proved exactly for bipartite lattices and arbitrary site spins by Lieb, Schultz and Mattis [52]. As pointed out in several papers the knowledge of the sign of the c_n is of great importance in different numerical methods, e.g. for the construction of variational wave functions [8,18,34,53], in quantum Monte-Carlo methods (which suffer from the sign problem in frustrated systems [54]) and also in the density matrix renormalization group method, where the application of the MPSR has substantially improved the method in a frustrated spin system [55].

For the J_1–J_2 model on the square lattice the violation of the MPSR was considered as one signal of destruction of magnetic LRO [8,9,12,13,18,34]. It was found that the MPSR (proved exactly only for $J_2 = 0$) survives till about $J_2 \approx 0.3 \ldots 0.4 J_1$. The exact Lanczos results for the ground state presented in references [8,9] and [12] were, however, restricted to systems of up to $N = 24$ sites. Here we present data for $N = 32$, 36, and 40 in Figure 6. From Figure 6 it is obvious that the MPSR is valid in very good approximation even till $J_2 \approx 0.4 J_1$. The MPSR starts to

be significantly violated beyond $J_2 = 0.4J_1$, where the Néel LRO breaks down.

3 Finite-size extrapolation

We use now our new data for $N = 40$ together with the known data for $N = 20, 32, 36$ to perform a finite-size extrapolation. Note that we do not include the data for the lattice with $N = 16$ sites. This lattice has an extra symmetry because it is equivalent to a hypercube in 4 dimensions. It was argued that, therefore, the $N = 16$ lattice exhibits an anomalous behavior [5]. The finite-size extrapolation rules for the two-dimensional HAFM are well known [56–60]. The extrapolation of the magnetic order parameters yields an estimate of the transition points between the semiclassically ordered phases (Néel and collinear) and the magnetically disordered quantum phase. In addition, since the scaling behavior is related to the low-energy degrees of freedom of the model, via the extrapolation procedure one can extract the J_2 dependence of other quantities such as the spin-wave velocity c and the spin stiffness ρ. It has been demonstrated that Lanczos data for finite lattices of up to $N = 36$ sites can provide quite accurate data for these quantities in the case of unfrustrated lattices [5,59,61].

In the seminal paper of Schulz et al. [5] the finite-size extrapolation procedure as well as some particular problems of the extrapolation appearing for the J_1–J_2 model were discussed in great detail. We follow here the lines of that paper, but do not repeat a detailed discussion of the extrapolation scheme.

We define the staggered magnetization, i.e., the Néel order parameter, as $m_0 = 2 \lim_{N\to\infty} M_N(\pi, \pi)$. The finite-size behavior of $M_N(\pi, \pi)$ is given by [5,56–58]

$$M_N^2(\pi,\pi) = \frac{1}{4} m_0^2 \left(1 + \frac{0.62075c}{\rho\sqrt{N}} + \cdots\right) \tag{3}$$

where c is the spin-wave velocity and ρ is the spin stiffness. The corresponding order parameter for the collinear LRO at large J_2 is defined as [5] $m_1 = \sqrt{8} \lim_{N\to\infty} M_N(\pi, 0)$. The finite-size behavior of $M_N(\pi, 0)$ is

$$M_N^2(\pi,0) = \frac{1}{8} m_1^2 + \frac{\text{const.}}{\sqrt{N}} + \ldots . \tag{4}$$

The results for m_0 and m_1 are shown in Figure 7. As expected we find a magnetically disordered GS phase around $J_2 = 0.5J_1$. The transition points are determined to $J_2^{c_1} = 0.35J_1$ and $J_2^{c_2} = 0.66J_1$, i.e., the range of the magnetically disordered GS phase obtained here is slightly larger than predicted, e.g., from series expansion [14,17,19,21] or coupled cluster approach [31]. For the unfrustrated square lattice HAFM ($J_2 = 0$) we obtain $m_0 = 0.621$ which is in good agreement with corresponding results obtained by other methods, e.g., 3rd order spin-wave theory ($m_0 = 0.6138$) [64], quantum Monte Carlo ($m_0 = 0.6140$) [63] or coupled cluster method ($m_0 = 0.6205$) [62].

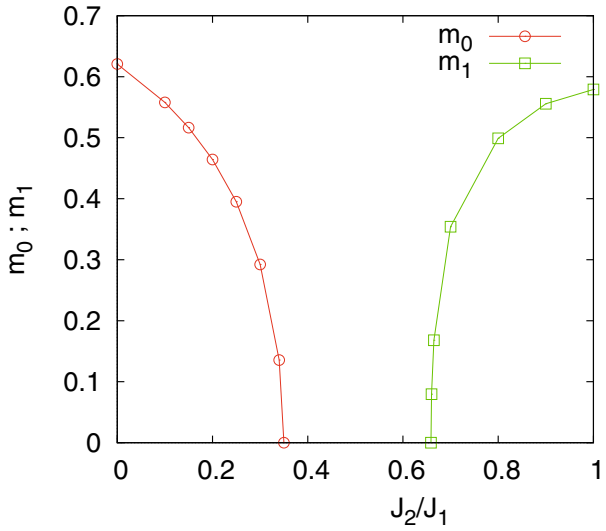

Fig. 7. (Color online) Order parameters m_0 (see Eq. (3)) and m_1 (see Eq. (4)) as a function of J_2/J_1.

The finite-size behavior of the GS energy is given by

$$\frac{E_{GS}(N)}{N} = e_0 - 1.4372 \frac{c}{N^{3/2}} + \ldots \tag{5}$$

The extrapolated energy e_0 is shown in Figure 8. Because of an irregular finite-size behavior near the maximum in e_0 (see inset in Fig. 8) the extrapolation becomes unreliable around $J_2 = 0.5J_1$ (this parameter region is indicated by the dotted line in the main panel of Fig. 8). Nevertheless, one can speculate that the kink in the extrapolated GS energy near $J_2 = 0.6J_1$ might be another hint for a first-order transition at $J_2^{c_2}$ between the semiclassical collinear phase and the quantum paramagnetic phase. The extrapolated GS energy, $e_0 = -0.6701$, for $J_2 = 0$ is again in very good agreement with corresponding results obtained by other methods, e.g., 3rd order spin-wave theory ($e_0 = -0.66931$) [64], quantum Monte Carlo ($e_0 = -0.66944$) [63] or coupled cluster method ($e_0 = -0.66936$) [62].

We can also perform a finite-size extrapolation of the gap to the first triplet excitation (spin gap) $\Delta_T(N) = E_0(S = 1) - E_{GS}(S = 0)$. The corresponding formula is

$$\Delta_T(N) = \Delta_T + \frac{a}{N} + \ldots \tag{6}$$

The results for Δ_T are shown in Figure 9. In the magnetically ordered Néel and collinear phases gapless Goldstone modes exist and consequently the spin gap should vanish. The finite values of the extrapolated gap for $J_2 < J_2^{c_1}$ and $J_2 > J_2^{c_2}$ give a hint of the limits of precision of the finite-size extrapolation of the spin gap. Nevertheless, it becomes obvious that there is a significant increase of Δ_T in the quantum paramagnetic phase $J_2^{c_1} < J_2 < J_2^{c_2}$. Note that for larger J_2 the energy scale of the system becomes proportional to J_2 that explains the increase in Δ_T with J_2 for $J_2 > 0.8$. A finite spin gap for $J_2^{c_1} < J_2 < J_2^{c_2}$ would be consistent with the findings of many papers

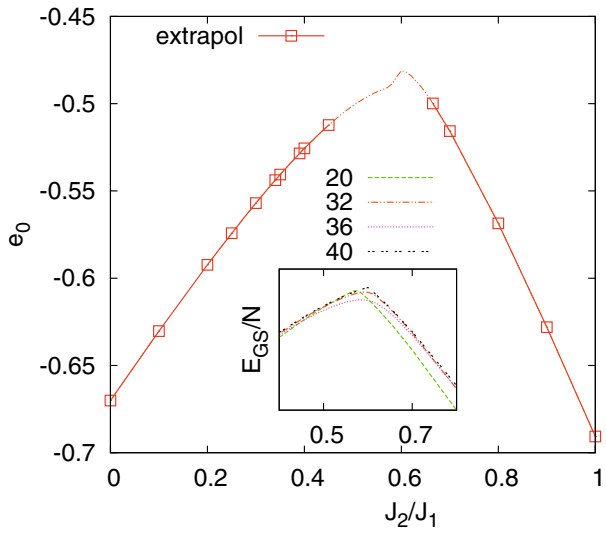

Fig. 8. (Color online) Ground-state energy per site. Main panel: Extrapolated value e_0 (see Eq. (5). Inset: Data for $N = 20$, 32, 36, and $N = 40$ around the maximum.

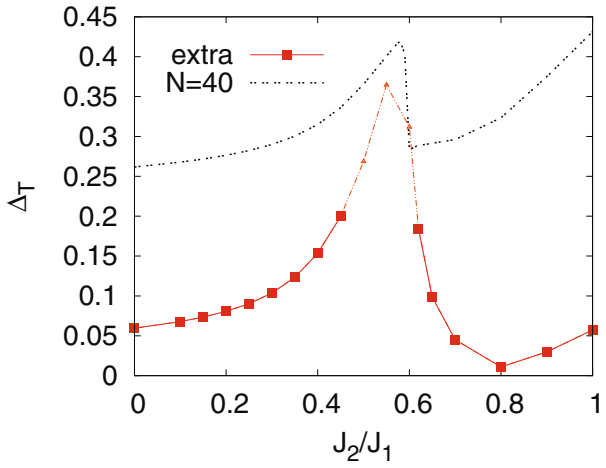

Fig. 9. (Color online) Spin gap Δ_T for $N = 40$ and extrapolated to $N \to \infty$ (see Eq. (6)).

which suggest that the quantum paramagnetic phase exhibits valence-bond order, see, e.g., references [21] and [31] and references therein. Note, however, that our finding is in contrast to recent DMRG studies on frustrated odd-leg ladders [26] where arguments for a gapless spectrum of the J_1-J_2 model on the square lattice have been given.

Next we consider the uniform susceptibility χ which is related to the spin gap by $\chi(N) = N\Delta_T(N)$. For the finite-size extrapolation of the uniform susceptibility we use [5]

$$\chi(N) = \chi + \frac{b}{\sqrt{N}} + \cdots \;\; ; \;\; \chi(N) = N\Delta_T(N). \qquad (7)$$

The results for $\chi(N = 40)$ and the extrapolated value χ are shown in Figure 10. In a gapful quantum paramagnetic phase, i.e., for $J_2^{c1} < J_2 < J_2^{c2}$, χ should vanish. Indeed, we observe a vanishing of χ around $J_2 = 0.5J_1$. However, the J_2 parameter region where χ is zero is clearly

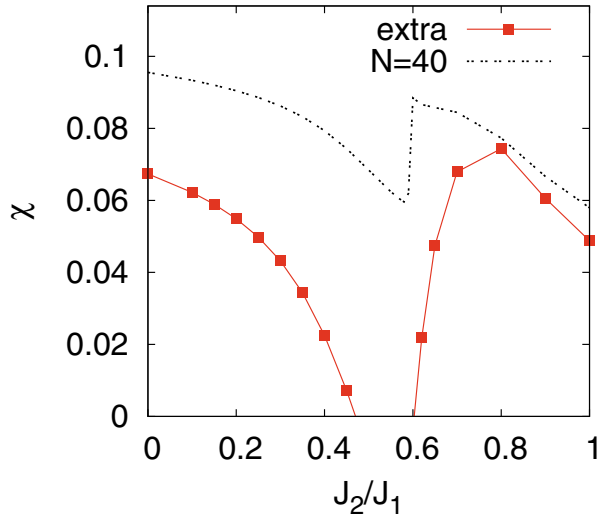

Fig. 10. (Color online) Susceptibility χ determined according to equation (7).

smaller than that where the order parameters m_0 and m_1 vanish. At $J_2 = 0$ we obtain $\chi = 0.0674$ which is in good agreement with data obtained by other methods, e.g., quantum Monte Carlo ($\chi = 0.0669$) [63], series expansion ($\chi = 0.0659$) [65], third-order spin-wave theory ($\chi = 0.06291$) [64], or coupled cluster method ($\chi = 0.065$) [66].

So far we have considered quantities which can be calculated directly for each finite lattice and for which the corresponding value for $N \to \infty$ is the leading term in a finite-size extrapolation formula, see equations (3, 4, 5, 6), and (7). A test of the accuracy the finite-size extrapolation is given by the comparison with best available data for the unfrustrated limit ($J_2 = 0$), see above. In addition to the direct calculation of certain magnetic quantities the finite size-extrapolation allows also an indirect determination of the spin-wave velocity c and the spin stiffness ρ which enter the finite size-extrapolation formulas (3) and (5) as prefactors of the leading finite-size corrections. First we can determine the spin-wave velocity c via equation (5). Using this result and also m_0 we find then the stiffness $\rho_1 \propto m_0^2 c$ via equation (3). Since ρ_1 is proportional to m_0^2, it vanishes at the same point $J_2^{c_2}$. Alternatively, we can use the hydrodynamic relation $\chi = \rho/c^2$, see, e.g., references [67] and [63], to determine the stiffness $\rho_2 = \chi c^2$. We show the spin-wave velocity and both values of the stiffness in Figure 11. Although, ρ_1 obtained via equation (3) and ρ_2 obtained via the hydrodynamic relation are quite different the qualitative behavior of both is similar to that obtained by direct calculation of ρ, e.g., using Schwinger boson [11] or coupled cluster approach [31]. The spin-wave velocity c also decreases with growing J_2. However, c remains finite at the magnetic-nonmagnetic transition at J_2^{c1} as predicted from the non-linear sigma model [67]. At $J_2 = 0$ we get $c = 1.287$, $\rho_1 = 0.1246$ and $\rho_2 = 0.1115$. These values are significantly lower than corresponding values obtained by quantum Monte Carlo method [63], 3rd order spin-wave

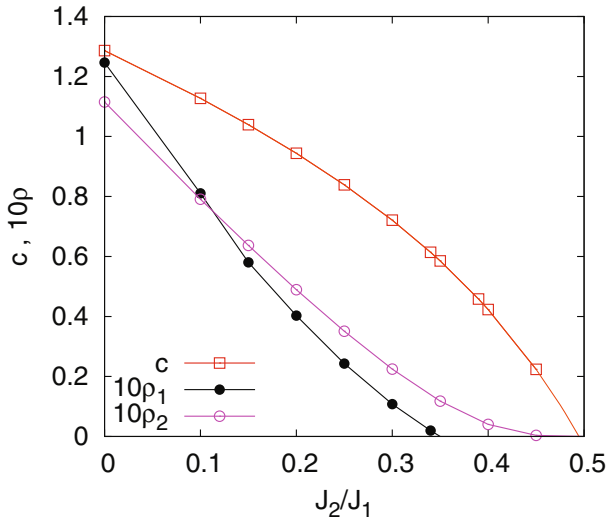

Fig. 11. (Color online) Spin wave velocity c and spin stiffness ρ. For better comparison ρ is multiplied by 10.

theory [64] or coupled cluster method [62,68]. Hence we may argue that the indirect determination of magnetic quantities via the prefactors of the leading finite-size corrections is less accurate.

4 Summary

In this paper we have presented detailed information on the GS and the low-lying excitations for the spin-1/2 J_1–J_2 HAFM on a finite square lattice of $N = 40$ sites. These data for the GS energy, the lowest triplet and singlet excitations, the spin-spin correlation functions and the magnetic order parameters may serve as benchmarks for approximate methods.

Including data for finite lattices of $N = 20, 32, 36$ sites we have performed finite-size extrapolations of several magnetic quantities. Using the well-known extrapolation formulas for the GS energy, the order parameters, the spin gap, and the uniform susceptibility we have determined these quantities for $N \to \infty$. To estimate the accuracy of the extrapolated quantities we have compared them with best available results for the unfrustrated limit $J_2 = 0$, where the high-order spin-wave theory and the quantum Monte Carlo method work well. At $J_2 = 0$ the extrapolated GS energy is in excellent agreement with spin-wave theory and quantum Monte Carlo results. The deviation of the Néel order parameter obtained by the finite-size extrapolation from the spin-wave and quantum Monte Carlo results is only about 1%.

Besides these quantities which have been determined directly for each finite lattice, in addition, we have used the formulas of finite-size extrapolation to determine the spin-wave velocity as well as the spin stiffness which appear in the prefactors of the leading finite-size corrections of the GS energy and the Néel order parameter. This 'indirect way' to determine spin-wave velocity and stiffness, however, yields only qualitative agreement with known results.

From the extrapolated magnetic order parameters we find the transition point from the magnetically ordered Néel phase to the gapful quantum paramagnetic phase to $J_2^{c_1} \approx 0.35 J_1$ and transition point between the magnetically ordered collinear phase and the quantum paramagnetic phase to $J_2^{c_2} \approx 0.66 J_1$.

This work was supported by the DFG (Ri615/16-1).

References

1. P. Chandra, B. Doucot, Phys. Rev. B **38**, 9335 (1988)
2. E. Dagotto, A. Moreo, Phys. Rev. Lett. **63**, 2148 (1989)
3. F. Figueirido, A. Karlhede, S. Kivelson, S. Sondhi, M. Rocek, D.S. Rokhsar, Phys. Rev. B **41**, 4619 (1990)
4. T. Einarsson, H. Johannesson, Phys. Rev. B **43**, 5867 (1991)
5. H.J. Schulz, T.A.L. Ziman, Europhys. Lett. **18**, 355 (1992); H.J. Schulz, T.A.L. Ziman, D. Poilblanc, J. Phys. I **6**, 675 (1996)
6. N.B. Ivanov, P.C. Ivanov, Phys. Rev. B **46**, 8206 (1992)
7. J. Richter, Phys. Rev. B **47**, 5794 (1993)
8. K. Retzlaff, J. Richter, N.B. Ivanov, Z. Phys. B **93**, 21 (1993)
9. J. Richter, N.B. Ivanov, K. Retzlaff, Europhys. Lett. **25**, 545 (1994)
10. T. Einarsson, H.J. Schulz, Phys. Rev. B **51**, 6151 (1995)
11. A.E. Trumper, L.O. Manuel, C.J. Gazza, H.A. Ceccatto, Phys. Rev. Lett. **78**, 2216 (1997); L.O. Manuel, A.E. Trumper, H.A. Ceccatto, Phys. Rev. B **57**, 8348 (1998)
12. A. Voigt, J. Richter, N.B. Ivanov, Physica A **245**, 269 (1997)
13. R.F. Bishop, D.J.J. Farnell, J.B. Parkinson, Phys. Rev. B **58**, 6394 (1998)
14. R.R.P. Singh, Z. Weihong, C.J. Hamer, J. Oitmaa, Phys. Rev. B **60**, 7278 (1999)
15. L. Capriotti, S. Sorella, Phys. Rev. Lett. **84**, 3173 (2000)
16. L. Siurakshina, D. Ihle, R. Hayn, Phys. Rev. B **64**, 104406 (2001)
17. O.P. Sushkov, J. Oitmaa, Z. Weihong, Phys. Rev. B **63**, 104420 (2001)
18. L. Capriotti, F. Becca, A. Parola, S. Sorella, Phys. Rev. Lett. **87**, 097201 (2001)
19. R.R.P. Singh, Weihong Zheng, J. Oitmaa, O.P. Sushkov, C.J. Hamer, Phys. Rev. Lett. **91**, 017201 (2003)
20. T. Roscilde, A. Feiguin, A.L. Chernyshev, S. Liu, S. Haas, Phys. Rev. Lett. **93**, 017203 (2004)
21. J. Sirker, Z. Weihong, O.P. Sushkov, J. Oitmaa, Phys. Rev. B **73**, 184420 (2006)
22. M. Mambrini, A. Läuchli, D. Poilblanc, F. Mila, Phys. Rev. B **74**, 144422 (2006)
23. D. Schmalfuß, R. Darradi, J. Richter, J. Schulenburg, D. Ihle, Phys. Rev. Lett. **97**, 157201 (2006)
24. F. Krüger, S. Scheidl, Europhys. Lett. **74**, 896 (2006)
25. H.T. Ueda, K. Totsuka, Phys. Rev. B **76**, 214428 (2007)
26. F. Becca, L. Capriotti, A. Parola, S. Sorella Phys. Rev. B **76**, 060401 (2007)

27. T. Munehisa, Y. Munehisa J. Phys.: Condens. Matter **19**, 196202 (2007)
28. J.R. Viana, J.R. de Sousa, Phys. Rev. B **75**, 052403 (2007)
29. L. Isaev, G. Ortiz, J. Dukelsky, Phys. Rev. B **79**, 024409 (2009)
30. R.F. Bishop, P.H.Y. Li, R. Darradi, J. Schulenburg, J. Richter, Phys. Rev. B **78**, 054412 (2008)
31. R. Darradi, O. Derzhko, R. Zinke, J. Schulenburg, S.E. Krüger, J. Richter, Phys. Rev. B **78**, 214415 (2008)
32. T. Pardini, R.R.P. Singh, Phys. Rev. B **79**, 094413 (2009)
33. T. Yoshikawa, M. Ogata, Phys. Rev. B **79**, 144429 (2009)
34. K.S.D. Beach, Phys. Rev. B **79**, 224431 (2009)
35. V. Murg, F. Verstraete, J.I. Cirac, Phys. Rev. B **79**, 195119 (2009)
36. T. Kashima, M. Imada, J. Phys. Soc. Jpn **70**, 3052 (2001)
37. R. Melzi, P. Carretta, A. Lascialfari, M. Mambrini, M. Troyer, P. Millet, F. Mila, Phys. Rev. Lett. **85**, 1318 (2000)
38. H. Rosner, R.R.P. Singh, Z. Weihong, J. Oitmaa, S.-L. Drechsler, W.E. Pickett, Phys. Rev. Lett. **88**, 186405 (2002)
39. Y. Kamihara, T. Watanabe, M. Hirano, H. Hosono, J. Am. Chem. Soc. **130**, 3296 (2008)
40. T. Yildirim, Phys. Rev. Lett. **101**, 057010 (2008)
41. Q. Si, E. Abrahams, Phys. Rev. Lett. **101**, 076401 (2008)
42. F. Ma, Z.-Y. Lu, T. Xiang, Phys. Rev. B **78**, 224517 (2008)
43. T. Senthil, A. Vishwanath, L. Balents, S. Sachdev, M.P.A. Fisher, Science **303**, 1490 (2004)
44. T. Senthil, L. Balents, S. Sachdev, A. Vishwanath, M.P.A. Fisher, Phys. Rev. B **70**, 144407 (2004)
45. F. Alet, P. Dayal, A. Grzesik, A. Honecker, M. Koerner, A. Laeuchli, S.R. Manmana, I.P. McCulloch, F. Michel, R.M. Noack, G. Schmid, U. Schollwoeck, F. Stoeckli, S. Todo, S. Trebst, M. Troyer, P. Werner, S. Wessel, J. Phys. Soc. Jpn Suppl. **74**, 30 (2005)
46. J. Richter, J. Schulenburg, A. Honecker, in *Quantum Magnetism*, edited by U. Schollwöck, J. Richter, D.J.J. Farnell, R.F. Bishop, Lecture Notes in Physics **645** (Springer, Berlin, 2004), p. 85
47. A. Läuchli, J.C. Domenge, C. Lhuillier, P. Sindzingre, M. Troyer, Phys. Rev. Lett. **95**, 137206 (2005)
48. J. Richter, J. Schulenburg, A. Honecker, D. Schmalfuß, Phys. Rev. B **70**, 174454 (2004)
49. J. Schulenburg, A. Honecker, J. Schnack, J. Richter, H.-J. Schmidt, Phys. Rev. Lett. **88,** 167207 (2002); A. Honecker, J. Schulenburg, J. Richter, J. Phys.: Condens. Matter **16**, S749 (2004)
50. J. von Neumann, E. Wigner, Z. Phys. **30**, 467 (1929); L.D. Landau, E. Lifshitz, *Quantum Mechanics: Non-Relativistic* (Pergamon, Oxford, 1977)
51. W. Marshall, Proc. Roy. Soc. A **232**, 48 (1955)
52. E.H. Lieb, T.D. Schultz, Mattis D.C. Ann. Phys. (N.Y.) **16**, 407 (1961)
53. B. Edegger, V.N. Muthukumar, C. Gros, Advances in Physics **56**, 927 (2007)
54. H. De Raedt, A. Lagendijk. Phys. Rev. Lett. **46**, 77 (1981)
55. U. Schollwöck, Phys. Rev. B **58**, 8194 (1998)
56. H. Neuberger, T. Ziman, Phys. Rev. B **39**, 2608 (1989)
57. P. Hasenfratz, F. Niedermayer, Z. Phys. B: Condens. Matter **92**, 91 (1993)
58. A. Sandvik, Phys. Rev. B **56**, 11678 (1997)
59. D.D. Betts, H.Q. Lin, J.S. Flynn, Can. J. Phys. **77**, 353 (1999)
60. H.Q. Lin, J.S. Flynn, D.D. Betts, Phys. Rev. B **64**, 214411 (2001)
61. D.D. Betts, J. Schulenburg, G.E. Stewart, J. Richter, J.S. Flynn, J. Phys. A **31**, 7685 (1998)
62. J. Richter, R. Darradi, R. Zinke, R.F. Bishop, Int. J. Modern Phys. B **21**, 2273 (2007)
63. M.S. Makivic, H.-Q. Ding, Phys. Rev. B **43**, 3562 (1991); K.J. Runge, Phys. Rev. B **45**, 12292 (1992), B.B. Beard, U.-J. Wiese, Phys. Rev. Lett. **77**, 5130 (1996); J.-K. Kim, M. Troyer, Phys. Rev. Lett. **80**, 2705 (1998)
64. C.J. Hamer, Z. Weihong, P. Arndt, Phys. Rev. B **46**, 6276 (1992); Z. Weihong, C.J. Hamer, Phys. Rev. B **47**, 7961 (1993); C.J. Hamer, Z. Weihong, J. Oitmaa, Phys. Rev. B **50**, 6877 (1994)
65. Z. Weihong, J. Oitmaa, C.J. Hamer, Phys. Rev. B **43**, 8321 (1991)
66. D.J.J. Farnell, R. Zinke, J. Schulenburg, J. Richter, J. Phys.: Condens. Matter **21**, 406002 (2009)
67. S. Chakravarty, B.I. Halperin, D.R. Nelson, Phys. Rev. B **39**, 2344 (1989)
68. S.E. Krüger, R. Darradi, J. Richter, D.J.J. Farnell, Phys. Rev. B **73**, 094404 (2006)